Journal of South American Earth Sciences 112 (2021) 103563

Contents lists available at ScienceDirect

Journal of South American Earth Sciences

journal homepage: www.elsevier.com/locate/jsames

Cyclostratigraphic analysis of the early Cretaceous laminated limestones of the Araripe Basin, NE Brazil: Estimating sedimentary depositional rates

João M.P. Gomes [a,*], Aristóteles M. Rios-Netto [a,b], Leonardo Borghi [a,c], Ismar de Souza Carvalho [a], João G. Mendonça Filho [a,d], Lília D. Sabaraense [a], Bruno C. Araújo [c]

[a] Universidade Federal do Rio de Janeiro, Instituto de Geociências, Departamento de Geologia, Programa de Pós-Graduação em Geologia (PPGL), 21941-909, Rio de Janeiro, Brazil
[b] Universidade Federal do Rio de Janeiro, Instituto de Geociências, Departamento de Geologia, Laboratório de Micropaleontologia Aplicada (MicrA), 21941-909, Rio de Janeiro, Brazil
[c] Universidade Federal do Rio de Janeiro, Instituto de Geociências, Departamento de Geologia, Laboratório de Geologia Sedimentar (Lagesed), 21941-909, Rio de Janeiro, Brazil
[d] Universidade Federal do Rio de Janeiro, Instituto de Geociências, Departamento de Geologia, Laboratório de Palinofácies e Fácies Orgânica (LAFO), 21941-909, Rio de Janeiro, Brazil

ARTICLE INFO

Keywords:
Araripe Basin
Cyclostratigraphy
Paleoclimate

ABSTRACT

By the Early Cretaceous, the Araripe Basin (Northeastern Brazil) is interpreted as having gone through a phase of tectonic quiescence, during which rates of sediment accumulation were mostly modulated by climatic variations. The Crato Member (Santana Formation, upper Aptian of Araripe Basin) consists of gray calciferous mudstone and parallel-stratified micritic limestone deposited in a lacustrine environment. The present study applied the principles of cyclostratigraphic analysis in the uppermost carbonate unit of the Crato Member, which comprises laminated limestone displaying a characteristic cyclic alternation of pale to dark laminae, in order to estimate sediment accumulation rates by relating the depositional record with astronomical cycles of known periodicity. An 8.5 m thick limestone succession was analyzed in order to build a time series by using two distinct data sources, namely spectral gamma ray readings and color variation chart. Additionally, petrographic and organic composition analyses were performed to investigate if environmental changes have affected those parameters. Results indicate that darker laminae reflect periods with concentration of sulfite related to relatively anoxic water conditions. The time series analysis allowed for an identification of two different astronomical cycles: (1) Milankovitch cycles, ranging from 18.6 ky to 39.4 ky, resulting in an estimated depositional rate of 3.25 cm/ky, with a total of 261 ky for the deposition of the whole studied interval; (2) Suess solar cycles, ranging 180–200 years, with an estimated depositional rate of 3.3 cm/ky, and a total of 257 ky for the deposition of the same interval. Therefore, this multidisciplinary approach led to the identification of Milankovitch and Suess high frequency solar cycles, based on which it was possible to determine the rate of deposition as well as the time span involved in it.

1. Introduction

Geologic cyclic phenomena are very common in Earth's history, some of them remaining registered in the sedimentary record. Cyclic patterns identified in sedimentary successions are, in most cases, controlled by climate, which in turn, can be related to astronomical cycles. Gilbert (1895) was the first to recognize the cyclicity of the sedimentary controls in a rhythmic alternation of limestones and shales. Since then, numerous studies (e.g., Berger, 1977, 1978; 1988; Berger et al., 1992; Schwarzacher, 1993; Weedon, 2003) have built up the bases and concepts for Cyclostratigraphy. Bradley (1929) has pioneered the application of the method to lake deposits, demonstrating the record of solar and Milankovitch cycles in that environment. The main principle of Cyclostratigraphy is the interpretation of repetitive patterns in the sedimentary record and its correlation with astronomical cycles with known periodicities (Strasser et al., 2006). Due to the relatively high frequency of such phenomena, Cyclostratigraphy is hold a common tool to increase the resolution of stratigraphic time.

* Corresponding author.
E-mail address: joaompeg@gmail.com (J.M.P. Gomes).

https://doi.org/10.1016/j.jsames.2021.103563
Received 21 May 2021; Received in revised form 10 September 2021; Accepted 10 September 2021
Available online 17 September 2021

The Alagoas Stage (approx. Aptian) corresponds to a time interval with major environmental change in the Brazilian sedimentary basins, related to the genesis of relevant hydrocarbon reserves described as a fluvio-lacustrine system. Therefore, it is important to achieve an accurate chronostratigraphic framework for this interval. In the Araripe Basin (Northeastern Brazil) the Alagoas Stage outcrops in several sites, allowing the direct observation of this interval, and their use as analogues of coeval rocks that, in the marginal basins, are in the subsurface and in most cases in offshore areas. However, it should be noted that, regarding the Araripe Basin, Rios-Netto et al. (2012) report that the two lithostratigraphic units attributed to the Alagoas Stage (Rio da Batateira and Santana formations, *sensu* Ponte and Appi, 1990) only comprise a single palynomorph biozone, the P-270 Biozone described by Regali et al. (1974). This restriction of the biostratigraphic tool makes it important to apply the Cyclostratigraphy technique in the search for a high-resolution framework for this interval.

Considering this context, the present work aims (1) to test the hypothesis of climate control related to astronomical cycles in the deposition of the Crato Member which is a unit of the Santana Formation, (2) to identify the controlling cycles, besides (3) determining the rate and time involved in the deposition of the uppermost carbonate unit of the Crato Member that displays a characteristic cyclic alternation of pale to dark laminae. This uppermost unit, called by Neumann (1999) C6 unit, has a deposition time estimated by him of 200–500 thousand years. Considering this estimation, we used a multidisciplinary approach, involving gamma ray and color spectral analyses, in addition to petrographic and organic facies analyses to improve this estimation.

2. Geological setting and stratigraphy

2.1. The Araripe Basin

The sedimentary infill of the Araripe basin is subdivided into four tectono-sedimentary sequences delimited by regional unconformities, denoted as Paleozoic, pre-, syn- and post-rift "megasequences" (*sensu* Assine, 1992, 2007). The Paleozoic sequence corresponds to the Mauriti Formation (Beurlen, 1962) and to the Upper Ordovician/Lower Devonian; the pre-rift sequence is composed by the Brejo Santo (Gaspary and Anjos, 1964) and Missão Velha (sensu Ponte and Appi, 1990) formations, both these unit being assigned to the Dom João Stage, approximately corresponding to the Upper Jurassic; the syn-rift sequence corresponds to the Abaiara Formation (Ponte and Appi, 1990), Lower Cretaceous; the post-rift sequence, related to the Upper Createcous, is composed by the Rio da Batateira (Ponte and Appi, 1990), Santana (Beurlen, 1962) and Arajara (sensu Ponte and Appi, 1990) formations, besides the Exu Formation (sensu Ponte and Appi, 1990).

2.2. The Santana Formation

The Santana Formation (Beurlen, 1962) is mainly composed by shales and limestones deposited in a lacustrine environment with increasing marine influence. It is stratigraphically arranged as Crato, Ipubi and Romualdo members (Beurlen, 1962, 1971, 1971; Mabesoone and Tinoco, 1973; Ponte and Appi, 1990). The basal unit, Crato Member, is characterized by alternating dark mudstones and laminated limestones with an abundant fossiliferous content representing a carbonated lacustrine sequence. Conformably overlaying, the Ipubi Member is composed by mudstones intercalated with evaporites in discontinuous layers corresponding to the evaporitic facies of the lacustrine system. The Romualdo Member is the topmost unit, which is classified as coastal lagoon gradually becoming proximal marine environment and is characterized by mudstones with the presence of fossiliferous calcareous concretions.

The Crato Member is composed by six carbonate packages separated laterally and vertically by mudstones forming an internal lake complex (Neumann, 1999). The present study focused in the uppermost carbonate unit of the Crato Member (namely C6 by Neumann, 1999) which comprises a profile of 10 m laminated limestones displaying a characteristic cyclic alternation of pale to dark laminae with 1–3 millimeters.

3. Materials and methods

3.1. Study area

The study area is part of the Araripe Basin, and hosts a well exposed laminated limestone succession showing a very characteristic cyclic pattern, with an alternation of pale and dark laminae in a millimeter scale, which corresponds to the uppermost stratigraphic unit of the Crato Member (Fig. 1). This study was carried out at the Três Irmãos Quarry, located on the Nova Olinda - Santana do Cariri road, south of Nova Olinda, Ceará State, Brazil.

3.2. Material

An 8.5 m thick stratigraphic section was taken as representative of the studied area (Fig. 2, red line). Along that section, 41 multispectral gamma ray points were measured, with a 0.2 m sampling space distance. Samples were collected every 0.25 m using a hand drill (Fig. 3a,b,c). Petrographic analysis was carried out on eight of these samples (PTI-04, 06, 07, 09, 11, 13, 15 and 17), spaced 0.50 m part, all of them taken between approximately 1.20 and 6.20 m, an interval in which the lamination is better preserved (Fig. 2) and due to the homogeneity of the interval, these samples are representative of the entire profile. Additionally, an isolated sample (PTI-B; Fig. 3d) was collected outside the section, but clearly from the same sedimentary succession. It was chosen because its higher preservation condition of the lamination pattern. This procedure was necessary to obtain a high-resolution image to the color spectral analysis. This additional sample was also used for petrographic and organic facies analyses.

3.3. Method

This multidisciplinary study involved three different methods, which are described below.

3.3.1. Petrography

Petrographic analysis was performed in 9 samples (PTI B; 04; 06; 07; 09; 11; 13; 15; 17) taken from the Três Irmãos quarry, with two objectives: (a) to ensure that the isolated sample can be correlated with that quarry section and (b) to enable a paleoenvironmental interpretation of the pairs couplets of pale and dark laminae identified in both.

For this analysis a Zeiss AXIO Imager. A2m was used, in addition to a microscope-attached camera for photomicrographs. The labels were processed by Zeiss AxioVision LE 4.2 software, in the Laboratory of Applied Micropaleontology at the Federal University of Rio de Janeiro (MicrA/UFRJ). The laminae were distinguished according to matrix, grains and fabric, following Flügel (2004), to identify parameters which could characterize the observed cyclic pattern of dark and pale laminae.

3.3.2. Organic facies

Organic facies analyses aim to obtain information about environmental conditions based on the changes of organic content (Menezes et al., 2008). In order to support the paleoenvironmental interpretation, total organic carbon – TOC, total sulfur – TS, insoluble residue – IR, and palynofacies were performed separately on material collected on a pale and dark lamina in the sample PTI-B.

These analyses were carried out in the Palynofacies and Organic Facies Laboratory at the Federal University of Rio de Janeiro (LAFO/UFRJ). For the palynofacies analyses, the samples were prepared using the non-oxidative method described by Oliveira et al. (2004) to remove the mineral matrix and concentrate the kerogen. For TOC/TS/IR

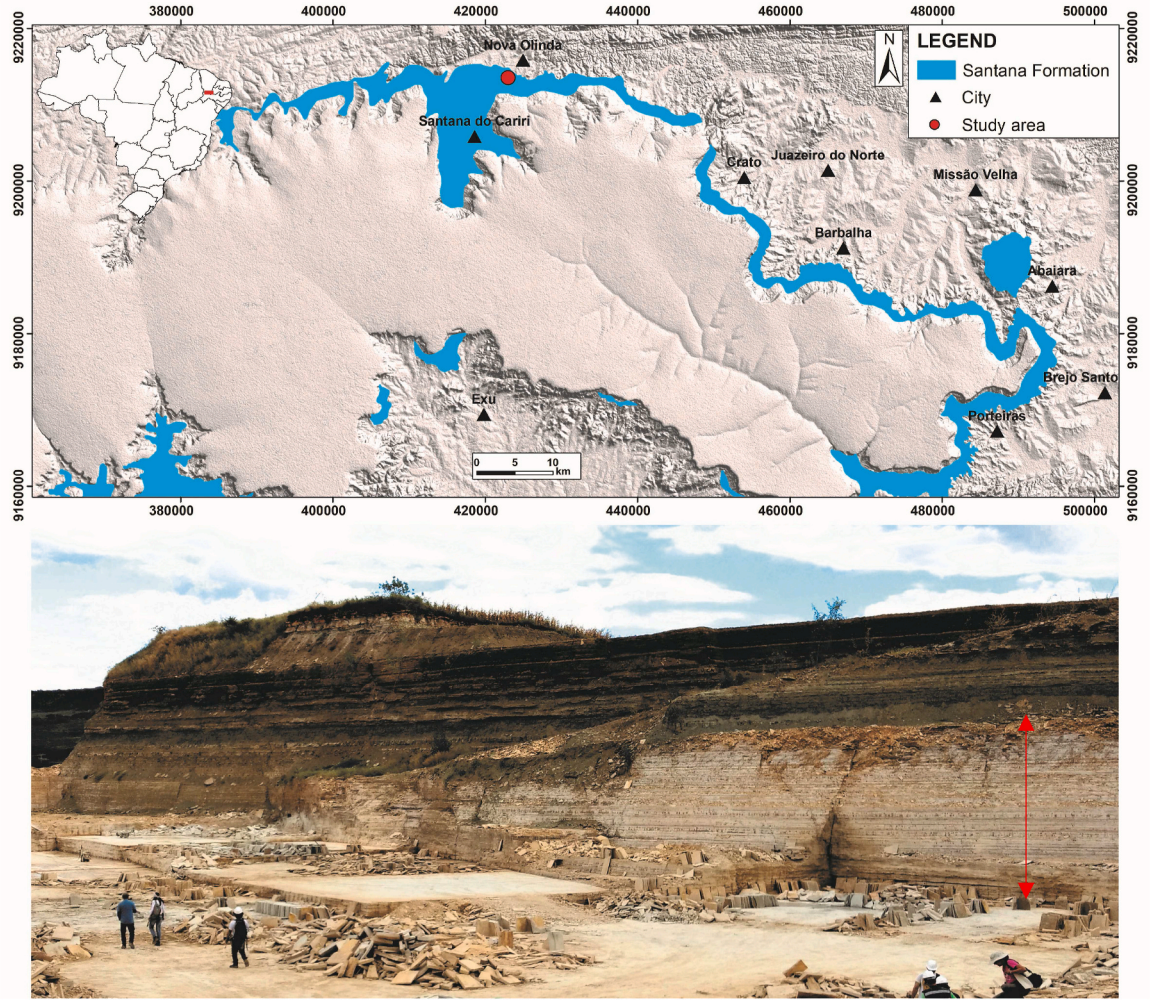

Fig. 1. Location of Três Irmãos Quarry (red dot) and the studied outcrop of laminated limestones (red line).

analyses, the material was prepared using the methods of ASTM D 4239 (American Society for Testing and Materials ASTM, 2008) and NCEA-C-1282 (Schumacher, 2002) to separate the insoluble residue and analyze it.

3.3.3. Spectral analysis

Concerning the spectral analyses, the present study followed a two-scale method: (a) first, in a meter scale, gamma ray spectral analysis was performed along the studied section; (b) second, in a millimeter scale, the color spectral analysis was done in the isolated sample (PTI-B). Gamma ray data was directly collected in the studied section by using a *Radiation Solutions RS-230 BGO Gamma-Ray Spectrometer Handheld.* For the color spectral analysis, the sample PTI-B was scanned with an EPSON GT-1500 Scanner; the colored image was converted to a gray scale image, which was subsequently converted to a gray scale log by using a code in Python.

The spectral analysis method involves the characterization of sequenced data within a time series (Priestley, 1981; Rayner, 2001). Any chemical or physical (visual) property displaying a cyclic pattern in a sedimentary succession (in which occurrence is repeated over same distance or time intervals) represents a time series (Schwarzacher, 1993; Cunha and Azambuja Filho, 2005; Anghinoni et al., 2019). This method allows for an identification of cyclic patterns and their correlation with astronomical cycles (Schwarzacher, 1993) through the identification of thicknesses of sedimentary cycles, that can be correlated to temporal patterns of astronomical cycles. In the present study the cycles considered for correlations were the Milankovitch cycles, long-term variations in solar radiation caused by the relative position of the Earth as to the Sun and the Moon, as well as the solar radiance cycles, short term variations (Table 1). Milankovitch cycles represent interactions among the Sun, Moon and Earth's orbit and Earth rotation itself, while the solar radiance cycle represent the cyclicity of solar activity. The amount of solar radiation that reaches the Earth is the most important factor that regulates climatic conditions (Schwarzacher, 2000). The average annual insolation for the whole Earth depends exclusively on the distance between the Earth, the Sun, and the solar constant, which is believed to been practically unchanged (Schwarzacher, 2000).

According to the Milankovitch theory the variation of the Earth's orbit determines the amount of radiation and therefore, the climate. The Milankovitch cycles predict constant orbital cycles, therefore, predicts a constancy of determined cyclic frequencies occurrences.

Climatic cycles are originated by the interaction of Earth's orbital parameters, eccentricity, precession, obliquity, and these cycles alter periodically the Earth's seasonal insolation, what would be registered as phase shifts in the geologic history.

Eccentricity determines the distance between the Earth orbit and the Sun. The eccentricity is known to vary within time, becoming sometimes more circular, and sometimes, more elliptical. Changes in orbital eccentricity rely on two main cycles. The major cycle shows variations at intervals near 413,000 years. The minor cycle presents variations near 100,000 years, but indeed, it consists of four cycles of nearly equal strength and periods varying between 95,000 and 131,000 years, that blend into a cycle around 100,000 years. These changes in the Earth-Sun distances varies the amount of solar radiation received by the Earth,

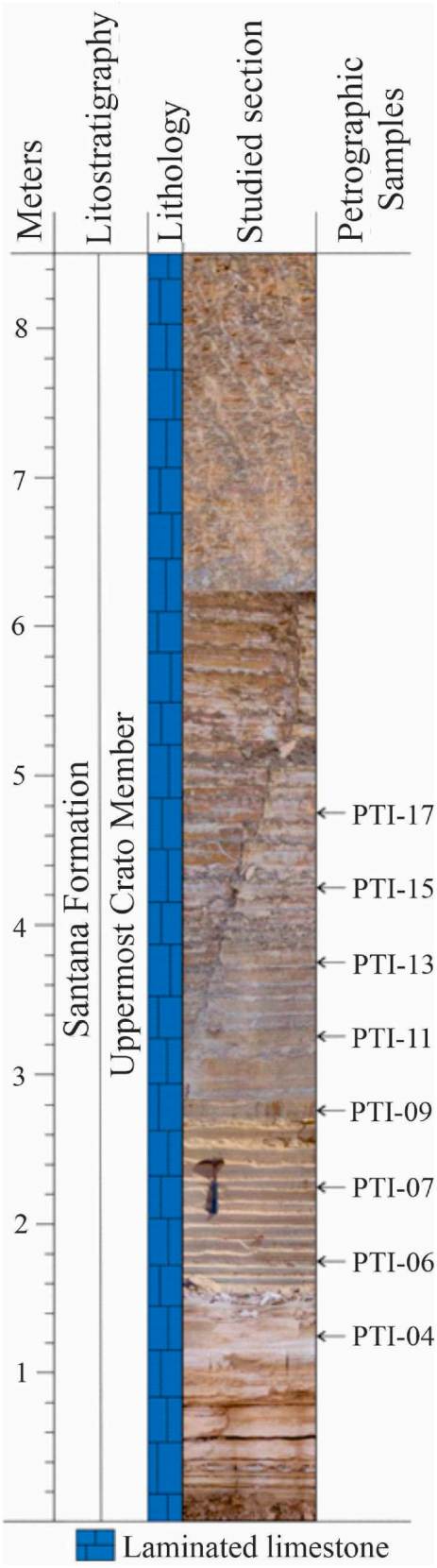

Fig. 2. Composite stratigraphic section taken in the laminated limestone of the Crato Member at the Três Irmãos Quarry, showing the positioning of the petrographic samples.

when at the perihelion, closest position from the Sun, it receives more radiation, when at the aphelion, farthest position from the Sun, it receives less radiation.

The precession motion of the Earth comprehends predominantly two motions. The axial precession is the Earth wobbling motion, caused by the gravitational pull of the Sun and the Moon. Its full rotation of Earth's axis through a circular path occurs every 25,700 years. Another kind of precession motion is known as the precession of the ellipse, which constrains the entire elliptical orbit of the Earth rotation, with long and short axes of the ellipse turning slowly in space. This motion is known to take near 19,000 year to repeat itself. These combined motions are responsible for the precession of equinoxes. The combined effects of the precession motions cause the solstices and equinoxes around Earth's orbit. Eccentricity has an important role over the effect of precession, on the amount of solar radiation received by the Earth.

Obliquity is the angle between Earth's equatorial plane and the plane of its orbit around the Sun, also equivalent to the angle between Earth's rotation and a line perpendicular to its rotation axis around the Sun. The obliquity is observed as the variation of this tilt angle, it varies ~ 3°. The decrease in the tilt tend to diminish the amplitude of seasonal differences. The increase of the tilt angle turns the polar region towards to the Sun in the summer, and it turns the poles away from the Sun in the winter season. Higher tilts produce more insolation at both poles. The obliquity is not evident at lower latitudes (Ruddiman, 2008). Changes in the tilt angle mainly amplify or soothe the seasons, particularly at the poles. The spectral analysis do not explain the possible connection between the climatic variations e the composition of the sediments, but it can provide evidences that connection existed (Weedon, 2003). If the connection between the environment history and the assumed astronomic signal exists, it is reasonable to expect that the frequency content of both curves to be comparable, however, the fluctuation of depositional rates and/or other geologic processes might incorporate a noise to the original signal (Schwarzacher, 1989).

The method of spectral analysis used in this study followed the one proposed by Perlmutter and Azambuja Filho (2005), which demands a stratigraphic interval that has sedimentary cycles of relatively uniform thickness, is described below.

The spectral analysis consists in detecting the dominant frequencies of a temporal series. As a mathematical artifact, the selected stratigraphic interval (i.e., gamma ray and color data) is the series input data, once it is resultant of a time series. The determination of a series periodogram allows one to estimate the power spectral density of the series. The periods determined, divided by the accumulation rate, will then result in a temporal series.

First, it is necessary to convert the gamma ray and color data into a graph, named periodogram. This analysis was performed via *TIBCO Statistica*^{TM} software, which made it possible to apply the Fast Fourier Transform, an algorithm used to convert the original data into a frequency representation. A periodogram allows the recognition of the frequencies that controls the repetition of equal values (horizontal axis), and the frequency peaks (named "power density"; vertical axis). When a value of gamma ray or gray scale is repeated periodically with a high density, the periodogram theoretically shows a peak that represents this frequency. The identified frequency peaks in the periodogram were then converted into thicknesses by the division of the sampling interval (0.2 m and 0.2 cm for gamma ray and color interval analysis, respectively) by the peak frequencies. These thicknesses represent the periodicity with which equal values of gamma or gray scale repeat along the interval.

After the values of thicknesses were obtained, the forwarding step was to correlate them with astronomical cycles. To do so, a technique of matrix similarity was applied, in which matrices of the identified thicknesses and astronomical cycles were compared in order to detect values with similarities greater than 95 %. Then, it was possible to correlate thicknesses with astronomical cycles and thus obtain results regarding depositional rates as well as the time span involved in it.

However, not every correlation between thicknesses and cycles with

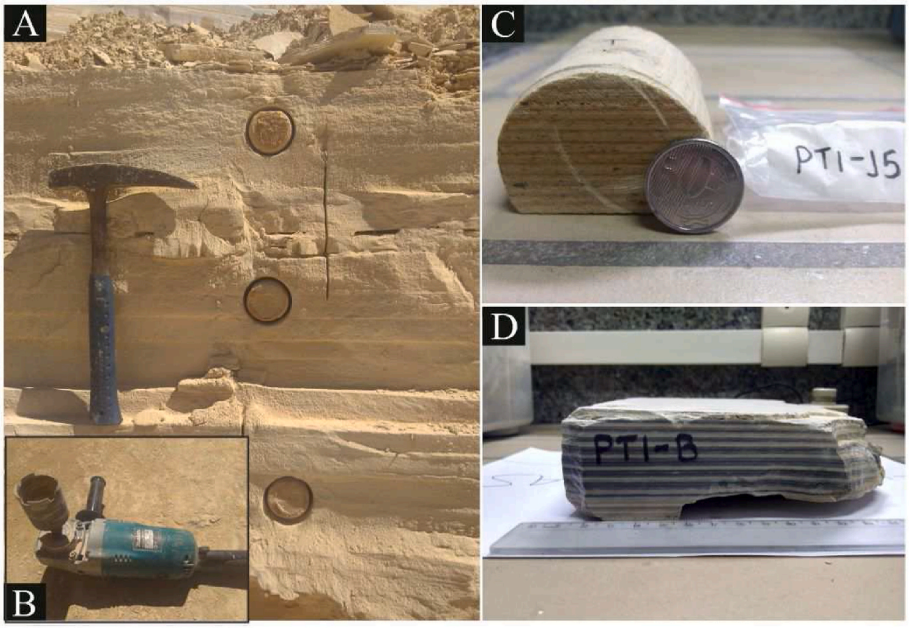

Fig. 3. The studied section was originally sampled every 0.25 m (A), using a hand drill (B), but the analyses were performed only every 0.50 m, considering the relative homogeneity of the interval. The same lamination pattern occurs both in the samples collected in the studied section and in the isolated sample, collected outside it, as can be seen in "C" (sample PTI-15) and in "D" (sample PTI-B).

Table 1
List of Milankovitch and solar cycles considered for the spectral analysis and its evidences (Adapted from Silva and Azambuja Filho, 2005).

Milankovitch cycles		
Cycle	Considered periods (ky)	Evidences
Precession	18.6 to 22.5	Rotation of Earth's axis
Obliquity	39.4 to 51.2	Angular variation of Earth's axis
Exccentricity	100 to 410	Variation of Earth's orbit around Sun
Solar cycles		
Cycle	Considered periods (years)	Evidences
Hale (Magnetic)	22	Sunspots
Double Hale	44	Sunspots
Gleissberg	80 to 100	Sunspots
Suess or de Vries	180 to 200	Correlation of ^{14}C,^{16}O and ^{18}O and sunspots
–	280	Evaporation/Precipitation Rates (Holocenic lakes)
–	650	Paleotemperatures
–	750	^{14}C and paleotemperatures
–	1000	^{14}C and paleotemperatures

a similarity greater than 95 % should be used. Studies about sedimentary rhythms in lakes give some ranges of acceptable depositional rates. In the case of a succession composed by an alternation of calcite and humic matter from the Cretaceous, it was calculated a range of 0.2 and 30 cm/ky by Glenn and Kelts (1991). In addition to this, an estimation of the Crato Member succession made by Neumann (1999) indicates that each of the six packages of the lake expansion has an estimation time of deposition of 200 thousand years to 500 thousand years based on the data regarding the tectonic evolution by Ponte Filho (1992). So, even in correlations of cycle/thicknesses greater than 95 %, some of them were discarded based on the results of these works.

4. Results

4.1. Petrographic description and interpretation

The petrographic description was performed in this work with a goal to identify cyclic pattern. The samples PTI-B; 04; 06; 07; 09; 11; 13; 15 showed the same alternation of two different laminae with the same microstructures (Table 2), confirming that the sample PTI-B can be correlated to that section. The main criterion used to distinguish the laminae was the microstructure, one being crenulated and the other plan-parallel. Other characteristics were not used as a distinctive criterion, since no repetitive pattern was identified. The microfabric of the samples is a laminated matrix, consisting of a homogenous micrite with sharp boundaries between the laminations showing an abrupt change in the color. The two distinct laminae defined on microscopic analysis, coincide with the alternating lamination recognized macroscopically in the studied section as an alternation of light and dark laminae.

4.1.1. Crenulated lamination (Cl)

These laminae were characterized by its dark color and crenulated lamination, with thickness varying between 0.92 and 4.96 mm (3 mm average; Fig. 4A–B). The main component is micrite, with a high concentration of pyrite (Fig. 4C). Precipitation of micrite grains in an anoxic environment was probably the process that formed these laminae.

Table 2
Petrographic features recognized in both studied section and in the isolated sample.

Petrographic features	Code	Diagnosis	Interpretation
Crenulated lamination	Cl	Limestone with irregular and dark lamination and high concentration of pyrite	Limestone formed by precipitation of carbonate grains with a high concentration of pyrite
Plan-parallel lamination	Ppl	Limestone with planar and pale laminae	Limestone formed by precipitation of carbonate grains

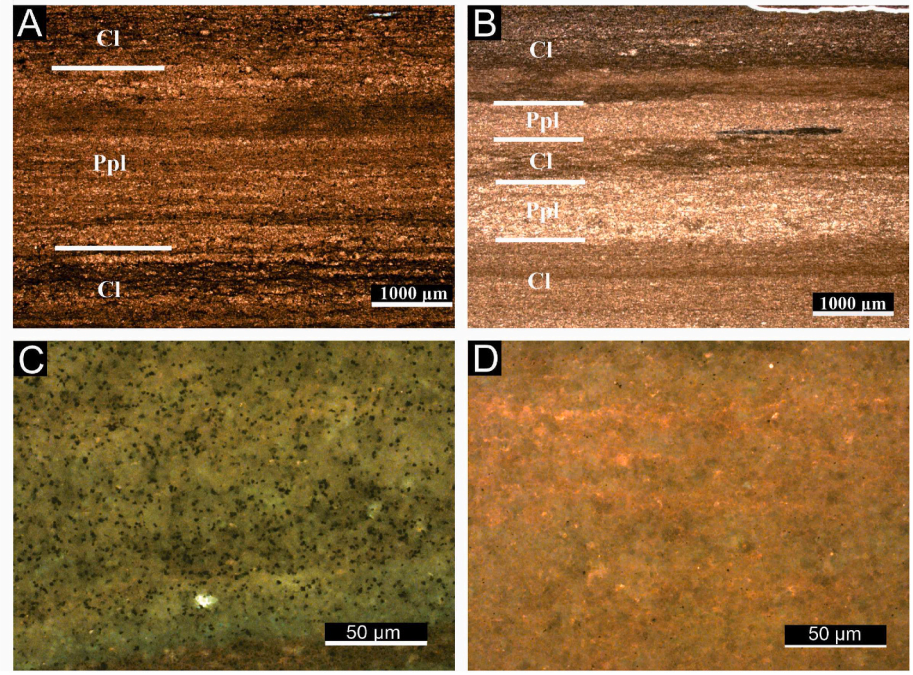

Fig. 4. Petrographic analysis: (A) alternation of the two laminations - sample PTI-04; (B) alternation of the two laminations - sample PTI-07; (C) detail of crenulated lamination - sample PTI-B; (D) detail of plan-parallel lamination - sample PTI-B. A and B: parallel nicols (10x); C and D: fluorescence (63 mm).

4.1.2. Plan-parallel lamination (Ppl)

These laminae have as a main characteristic its pale color and planar lamination, in contrast with the Cl lamination (Fig. 4A–B). These laminations vary between 0.79 and 3.51 mm with a 2.5 mm average. Micrite is also the main component, but pyrite is absent (Fig. 4D). The process that originated these laminae was probably the precipitation of micrite in a more oxic environment.

4.2. Organic facies

The dark lamina and the pale lamina from the PTI-B sample showed that both laminae present similar organic composition: phytoclasts, sporomorphs (mainly as tetrads of spores and clusters of pollen grains) and bacterial amorphous organic matter (AOM). The percentage of organic components is also very similar in both types of laminations, with a remarkable predominance of bacterial AOM (more than 90 %). However, despite the similarity of organic composition in both qualitative and quantitative analyses, it was possible to observe a great amount of pyrite agglomerates, mainly as framboidal pyrite, impregnating the matrix of AOM in the dark laminae, suggesting that the occurrence of this mineral as the most probable explanation for its dark color. Fig. 5 shows the differences in the bacterial AOM of the two laminations, attributed to the presence of pyrite only in the dark laminae, since the phytoclasts and sporomorphs were the same in both

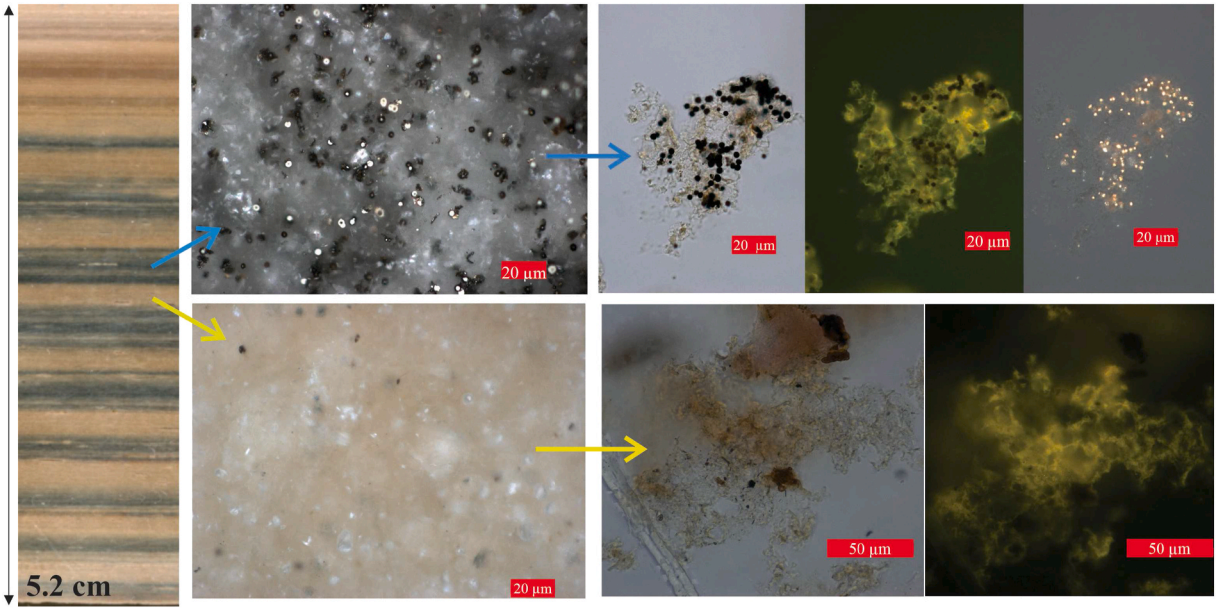

Fig. 5. AOM found in the dark and the pale laminae of the sample PTI-B. Blue arrow indicates the pelicular bacterial AOM from the dark lamination with a high concentration of pyrite. Yellow arrow points to the pelicular bacterial AOM from the pale laminae without pyrite.

laminations.

The TOC content is these laminae was very similar varying between 0.28 wt % (dark laminae) and 0.33 wt % (pale laminae) as well as the $CaCO_3$ content (99.7 wt % in the dark laminae and 99.9 wt % in pale laminae). However, sulfur content was higher in dark laminae (0.43 wt %) than in pale colored laminae (0.06 wt %) and sporomorphs content was higher in pale laminae (4.37 wt %) than in dark colored laminae (2.37 wt %).

The similarities and differences observed in the organic content and pyrite occurrence and concentration suggests a climatic variation during the deposition of the analyzed carbonatic sequence, mainly related to alternation of dryer and wetter conditions, as well as redox conditions.

4.3. Gamma ray spectral analysis

The gamma ray log along with the uranium, thorium and potassium logs of the studied section are presented in Fig. 6 and the corresponding periodogram (based on the gamma ray log) is presented in Fig. 7. The periodogram presents the intensity that each discrete frequency contributes with the total process variance. The higher is the intensity of the power spectrum, higher is the importance of the associated interval to that frequency on the series. The ratio between the sampling distance and the power spectrum frequencies provided the thicknesses, for each of the red dots frequencies. Tables 3 and 4 show the matrices of the Milankovitch cycles (built with the periods shown at Table 1) and the matrix of calculated thicknesses (built from the thicknesses identified at the periodogram, Fig. 7), respectively.

In order to correlate astronomical cycles and thicknesses intervals, the matrices similarity was performed by comparing the results of the ratios of the two matrices. Once finding two numbers with at least 95 % of similarity, it was possible to correlate the astronomical cycle and the thickness that resulted from those two ratios. For example, once the values of 1.75 (from Milankovitch matrix) and 1.66 (from thicknesses matrix) showed more than 95 % of similarity, then the 39.4 thousand years cycle can be correlated with the 1.33 m thickness and the 22.5 thousand years cycle, with the 0.8 m thickness. By identifying similarities between the matrices, it was possible to correlate the periodicity of the Milankovitch cycles and thicknesses (Table 5), as following:

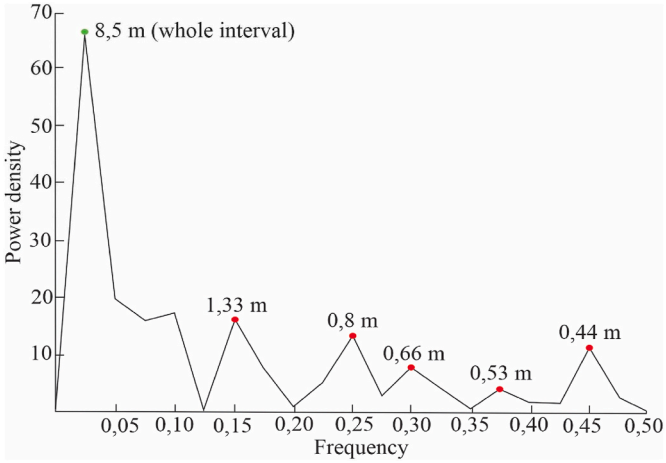

Fig. 7. Periodogram of the gamma ray log. Red dots indicate the thicknesses used for spectral analysis and green dot indicate the representation of the entire interval.

Table 3
Matrix of the Milankovitch cycles. The values referring to periodicity of the cycles were divided among themselves ("y" axis/"x" axis) and the obtained ratios were used to compare with the ratios obtained between the thicknesses identified in the periodograms (Silva and Azambuja Filho, 2005).

Milankovitch matrix (ky)						
	410	100	51.2	39.4	22.5	18.6
410	1	4.10	8.00	10.41	18.22	22.04
100		1	1.95	2.54	4.44	5.38
51.2			1	1,29	2.27	2.75
39.4				1	1.75	2.12
22.5					1	1.21
18.6						1

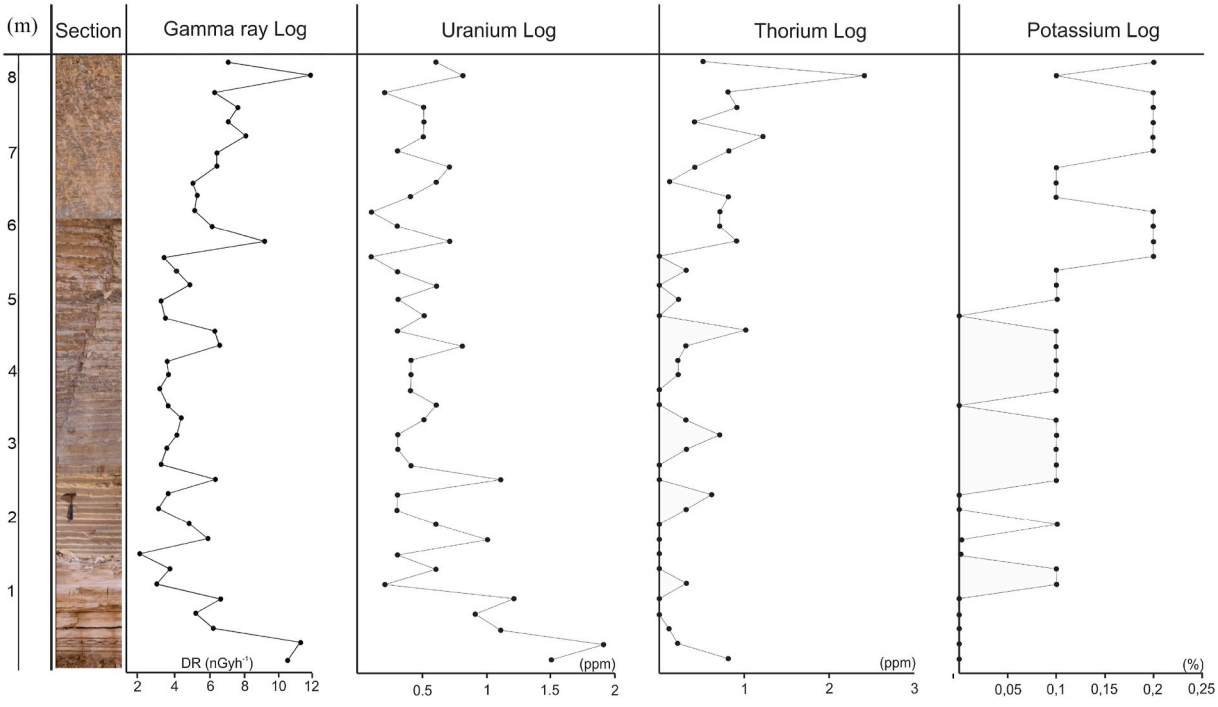

Fig. 6. Gamma ray, uranium, thorium and potassium logs along the studied section.

Table 4
Matrix of the identified thicknesses. The values referring to identified thicknesses were divided among themselves ("y" axis/"x" axis) and the obtained ratios were used to compare with the ratios of the periodicity of the cycles.

Thicknesses matrix (m)					
	1.33	0.80	0.66	0.53	0.44
1.33	1	1.66	2.02	2.51	3.02
0.8		1	1.21	1.51	1.82
0.66			1	1.25	1.50
0.53				1	1.20
0.44					1

Table 5
Results for gamma ray spectral analyze with the thicknesses being related to the cycles and its depositional rates.

Thicknesses (m)	Corresponding Milankovitch cycle (ky)	Depositional rates (cm/ky)
1.33	39.4 (obliquity)	3.38
0.8	22.5 (long precession)	3.56
0.66	18.6 (short precession) to 22.5 (long precession)	2.93 to 3.55
0.53	18.6 (short precession)	2.85
Average depositional rate: 3.25 cm/ky		
Span of time for the deposition of the entire section (8.5 m): 261 ky		
Amount of precession cycles represented in the entire section: 13		

(1) the thickness of 1.33 m was correlated to the cycle of obliquity (39.4 ky);
(2) the thickness of 0.8 m was correlated to the long cycle of precession (22.5 ky);
(3) the thickness of 0.66 m was correlated to the long (22.5 ky) and short (18.6 ky) cycles of precession, indicating a variation of depositional rate;
(4) the thickness of 0.53 m was correlated to the short cycle of precession (18.6 ky);
(5) the thickness of 0.44 m could not be linked to any of the Milankovitch cycles because of its higher frequency.

Beside those results, Table 5 also presents the estimate duration and deposition rate for each thickness, the average depositional rate, how much time was involved in the deposition of the whole section, and how many precession cycles were represented in the entire section.

4.4. Color spectral analysis

Fig. 8 shows the original-colored image of the sample PTI-B laminae, the grayscale image of those laminae, and the grayscale log generated by a Python code, while Fig. 9 presents the corresponding periodogram. Tables 6 and 7 present the matrices of the solar cycles (built with the periods shown at Table 1) and the calculated thicknesses (built from the thicknesses identified at the periodogram on Fig. 9), respectively.

Using the same method of matrix similarity, it was possible to correlate the periodicity of the solar cycles and thicknesses by

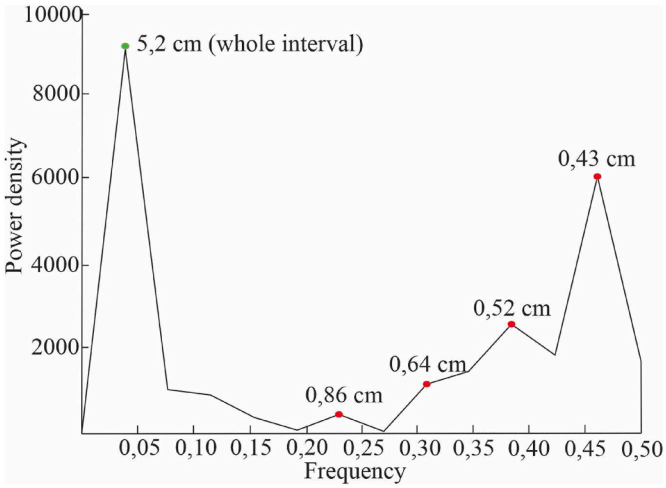

Fig. 9. Periodogram for gray scale profile. Red dots indicate the thicknesses used for spectral analysis and green dot indicates the representation of the entire section.

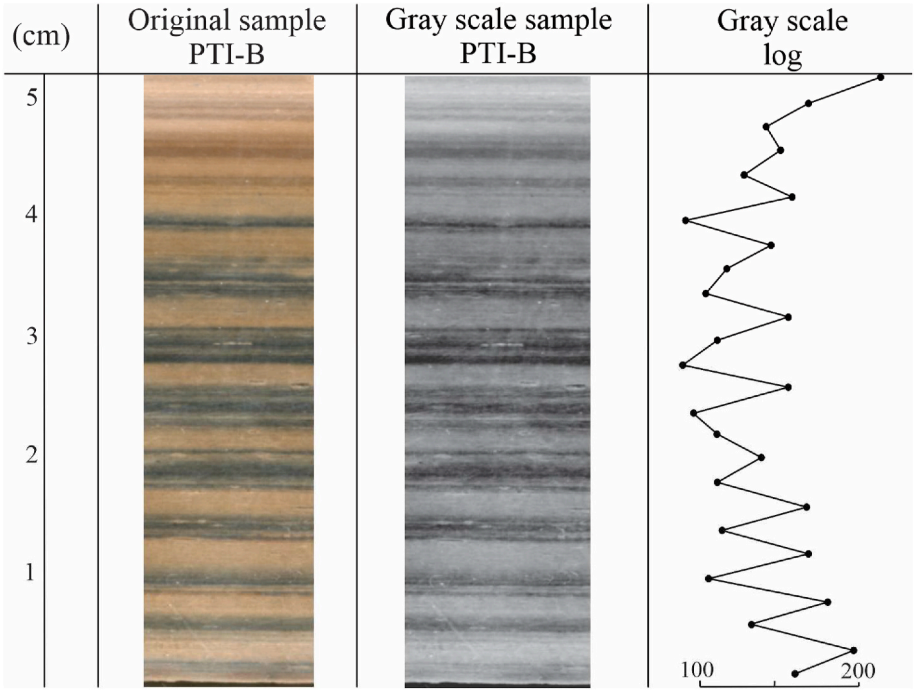

Fig. 8. Sample PTI-B converted to a gray scale image and its correspondent gray scale log used for color spectral analysis.

Table 6
Matrix for solar cycles. The values referring to periodicity of the cycles were divided among themselves ("y" axis/"x" axis) and the obtained ratios were used to compare with the ratios obtained between the thicknesses identified in the periodograms (Silva and Azambuja Filho, 2005).

Solar cycles matrix (years)										
	1000	750	650	280	200	180	100	80	44	22
1000	1	1.33	1.54	3.57	5.00	5.56	10.00	12.50	22.73	45.45
750		1	1.15	2.68	3.75	4.17	7.50	9.38	17.05	34.09
650			1	2.32	3.25	3.61	6.50	8.13	14.77	29.55
280				1	1.40	1.56	2.80	3.50	6.36	12.73
200					1	1.11	2.00	2.50	4.55	9.09
180						1	1.80	2.25	4.09	8.18
100							1	1.25	2.27	4.55
80								1	1.82	3.64
44									1	2.00
22										1

Table 7
Matrix from identified thicknesses. The values referring to identified thicknesses were divided among themselves ("y" axis/"x" axis) and the obtained ratios were used to compare with the ratios of the periodicity of the cycles.

Thicknesses matrix (cm)				
	0.86	0.64	0.52	0.43
0.86	1	1.34	1.65	2.00
0.64		1	1.23	1.49
0.52			1	1.21
0.43				1

comparing the matrices (Table 8), as following:

(1) the thicknesses of 0.86, 0.64 and 0.43 cm were correlated to the solar cycles of Suess (180–200 years);
(2) the thickness of 0.52 cm could not be linked to any of the solar cycles.

Additionally to those results, Table 8 also shows the estimate duration and deposition rate for every thickness, the average depositional rate, how much time was involved in the deposition of the whole section, and how many solar cycles of Suess were represented in the whole sample. Applying these results for the whole section of 8.5 m, the time of deposition estimated at ~257 ky.

5. Discussion

5.1. Validation between spectral analysis and geologic data

The spectral analysis presented in the present work was carried out using statistical techniques that associated numerical values of gamma ray and colors (gray scale) to known astronomical cycles. Therefore, for its validation, it is necessary to compare these results with geological information indicating paleoenvironmental conditions that support the climatic alternation suggested by the statistical study.

It is considered that this validation was given by the petrographic and organic facies analyses that are part of the present study, since the results of these analyzes made it possible to differentiate two environmental conditions, reflected by the absence and the occurrence of pyrite. The integration of gamma and color spectral analyses, petrographic and organic composition suggested a plausible link between the solar cycles of Suess and the lake conditions because the thicknesses (0.43, 0.64 and 0.86 cm) correlated to these cycles in the color spectral analyses are clearly related to a pair of a pale and a dark lamina in the sample PTI-B.

Table 8
Results for color spectral analyze with the thicknesses being related to the cycles and its depositional rates.

Thicknesses (cm)	Corresponding solar cycle (years)	Depositional rates (cm/ky)
0.86	200	4.30
0.64	200	3.20
0.43	180	2.39
Average of depositional rates: 3.3 cm/ky		
Span of time for the deposition of interval represented by the sample (5.2 cm): 1575 years		
Amount of Suess cycles in the whole sample: 8		

5.2. Milankovitch's cycles and its influence in deposition of the Crato Lake

In this study section different Milankovitch cycles were identified with a periodicity matrix comparison, as alternative tool, once there was no high-resolution gamma ray available. Based on this comparison, the full section allegedly represents 261,000 years of deposition, a timespan that respects the limits described by previous studies, in that each sequence would represent between 200 and 600 ky of deposition (Neumann, 1999). Considering the method assumptions, this study should be able to identify cycles of eccentricity, obliquity, and precession. Nonetheless, only cycles of obliquity and precession were identified. According to the calculated timespan of the section of 261,000 years, a cycle of short eccentricity would have been expected (cycle ~100,000 year).

As a validation test, the gamma ray was plotted against the different cycle's thicknesses (Fig. 10). Only some sections of the identified cycles seem to present similarities with the gamma ray profile, mostly between, perhaps the first meters. The cycle that presented some similarity with the gamma ray interval, seems to be the long precession cycle (0.8 m), in the first few meters its higher peaks are coincident with the nearby higher peaks of the gamma ray data, suggesting that this cycle might had some relationship with the higher values of the gamma ray data (mostly associated to the uranium log). The lack of gamma ray data in a proper resolution makes it difficult to evaluate the adjustment of the precession's cycles surfaces identified, or even to validate the analysis.

Regarding the ratios of the Milankovitch's matrix, presented at Table 3, it would be expected a given thickness to correspond to the eccentricity cycle. Relating these Milankovitch ratio matrix: the eccentricity/long precession ratio (ec/lp = 4.44), eccentricity/short precession ratio (ec/spr = 5.38) and eccentricity/obliquity ratio (ec/ob = 2.54) to the section identified thicknesses matrix, with the calculated values for the long precession (0.8 and 0.6 m), short precession (0.6 and 0.53 m), and obliquity (1.33 m), it would have provided the values of 2.66, 2.85, 3.37 and 3.5 m to be expected as plausible answers to the short eccentricity cycle (Fig. 11). A thickness in between those values should have been identified as correspondent to the eccentricity cycle surface since the depositional rate seems to have fluctuated along the section. The lack of this data identification seems to be a limitation given by the method, the interval, and/or the sampling interval used.

Some similarities can be noticed when comparing the gamma ray data plot with the 3.55 m thickness curve. The decrease of values in the

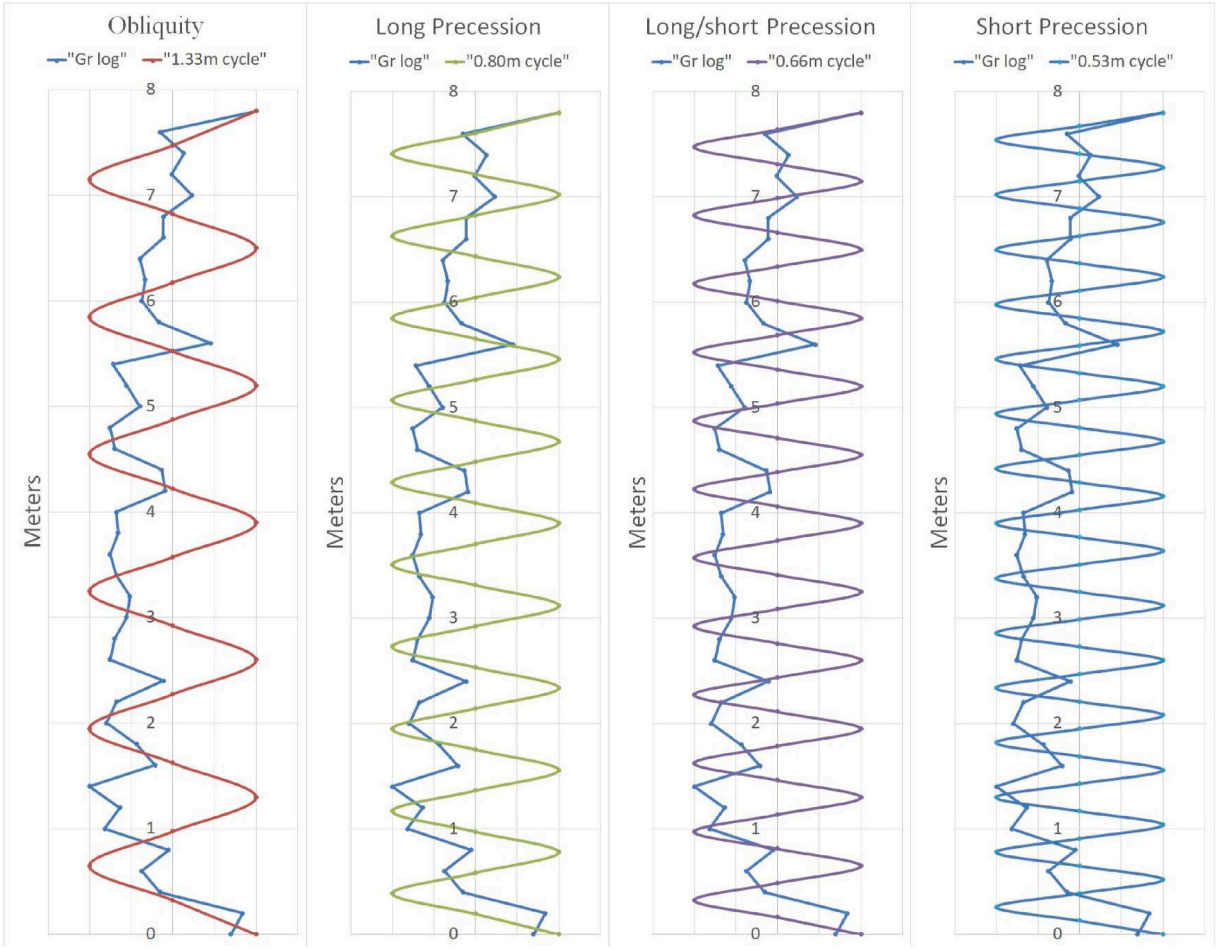

Fig. 10. Obliquity, long precession, long and short precession, and short precession sinusoidal curves for the calculated thicknesses along with the gamma ray log (Gr log).

first few meters, as such as, the increase of values at the top of the profile, both seem to fit into a 3.55 m cycle curve. The eccentricity controls the insolation of the Earth, as a main drive force, and for that, it modulates its rates of insolation that the Earth receives through time. As Fig. 11 show similarities between the 3.55 m thickness cycle and the general variation of the gamma ray, it could be plausible the adherence of the 3.55 m cycle curve to the short eccentricity cycle, even though, the analysis could not identify the frequency associated to these thicknesses, or by lack of samples, or by similarity with harmonic frequencies, or any other reason. It is suggested that a similar thickness might represent the geologic registry of the short eccentricity cycle, but further analyses such as high-resolution gamma ray analysis are needed in order to make proper assumptions.

5.3. Suess cycles and its influence in deposition of the Crato Lake

The most striking cyclical aspect of laminated limestones is the alternation between pale and dark laminae. It is a characteristic visible to the naked eye and that could be classified distinctively, both in petrography and in the analysis of organic facies. Each pair of pale and dark laminae is related to the Suess cycles of approximately 200 years.

The results of spectral analysis in the laminated limestones of the uppermost unit of Crato Member indicated both an influence of Milankovitch cycles and of the solar cycles with ranges of 180–200 years. However, although the Milankovitch cycles were identified, it is the Suess solar cycles that should be considered the main influence over the deposition of the limestones because of its higher frequency. These cycles, firstly identified by Suess (1980) based on correlations of ^{14}C with sunspots, were also reported by Kern et al. (2012), Novello et al. (2012), Seidenglanz et al. (2012) and Wagner et al. (2001). The influence of these cycles was identified not only on lake deposits, like in the researches from Hodell et al. (2001), Kern et al. (2012) and Schimmelmann et al. (2003), but also on speleothems (Novello et al., 2012) and tree rings (Ludecke et al., 2015; Raspopov et al., 2008). The recognition of this same periodicity in different kind of deposits at different locations with millions of years of difference could be considered as an indicative of external forcing that influenced over the deposition (Raspopov et al., 2008).

The same 200-year cycle pointed out by the cited authors, based on proxies as isotopic variation, magnetic susceptibility, and abundance of ostracodes, was recognized in the present work through the integration of the color spectral, organic facies and petrographic analyses.

The paleoenvironmental conditions interpreted from the organic facies analyses in the pair of laminae have indicated fluctuations in water balance that could have impacted salinity during periods of higher precipitation and evaporation, characterizing the “Crato lake” as an ectogenic meromixis lake. This condition is present when occurs an inflow of fresh water in saline water, or vice-versa (Walker and Likens, 1975). As can be deduced from our results, the alternation of pale and dark laminae probably corresponds to the inflow of fresh water in saline water in the “Crato lake”. Then, the cycle of approximately 200 years could be divided in two phases: (1) the first phase with a more anoxic lacustrine environment (deposition of Cl lamination), associated with a concentration of ions and reduction of sulfate forming pyrite, and (2) a second phase corresponding to a period of a more oxic lake, with inflows of fresh water, associated with a pause in the reduction process

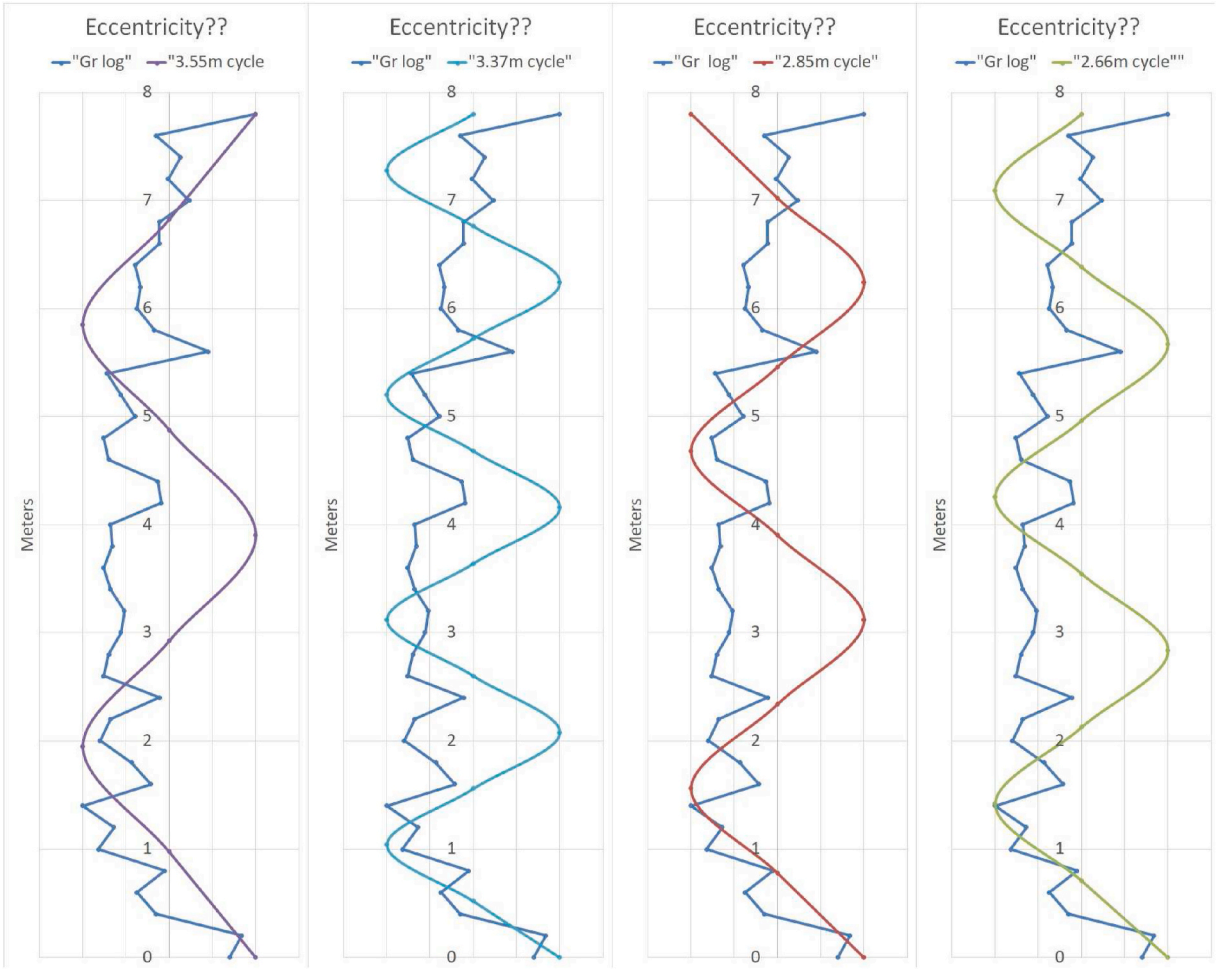

Fig. 11. Eccentricity cycle surfaces calculated long with the gamma ray log (Gr log).

(deposition of Ppl lamination).

6. Conclusions

The cyclostratigraphic analyses in the laminated limestones succession corresponding to the uppermost unit of Crato Member was performed in a two-scale study using gamma ray and color spectral analysis in addition to petrographic and organic facies analyses. This multidisciplinary study allowed the identification of climate control on the deposition of that unit with the influence of two types of astronomical cycles over this unit, the Milankovitch and the Suess solar cycles.

The use of the spectral analysis, correlating the periods of those astronomical cycles and the thicknesses, made it possible to determinate the rate and time involved in the deposition of the Crato Member. The average depositional rate for the 8.5 m profile was calculated in 3.28 cm/ky with a depositional time of 260 thousand years. The Milankovitch's identified cycles curves did not match properly the gamma ray log, what made difficult to evaluate the similarity between the profiles. The gamma ray data in a higher resolution could perhaps identify and evaluate a better adjustment of the Milankovitch's cycles and validate the analysis.

Along with it, it was possible to estimate that a pair of pale and dark laminae from that same succession has a depositional time of 200 years being related to the Suess solar cycles.

In addition to those results it was possible to suggest some paleoenvironmental conditions: (1) Dark laminae indicates more anoxic periods because of the high concentration of pyrite and; (2) Pale laminae indicates more oxic periods with a pause in redox conditions due the lack of pyrite.

Author statement

João M. P. Gomes: Conceptualization, Methodology, Software, Formal analysis, Investigation, Writing – Original Draft, Writing – Review & Editing, Visualization Aristóteles M. Rios-Netto: Conceptualization, Resources, Writing – Original Draft, Writing – Review & Editing, Visualization, Supervision, Project administration, Funding acquisition, Leonardo Borghi: Conceptualization, Resources, Project administration, Funding acquisition Ismar de Souza Carvalho: Conceptualization, Resources, Project administration, Funding acquisition João G. Mendonça Filho: Formal analysis, Resources, Writing - Original Draft, Lília D. Sabaraense: Formal analysis, Writing - Review & Editing, Bruno C. Araújo: Investigation, Resources, Supervision.

Declaration of competing interest

The authors declare that they have no known competing financial interests or personal relationships that could have appeared to influence the work reported in this paper.

Acknowledgments

The authors gratefully acknowledge the research & development project "Correlação estratigráfica, evolução paleoambiental e paleogeográfica e perspectivas exploratórias do Andar Alagoas", sponsored by Shell Brasil Petroleo Ltda. with resources allocated to R&D institutions

accredited by the Brazilian National Petroleum, Natural Gas and Biofuels Agency - ANP (technical cooperation agreement #20219-2).

References

American Society for Testing and Materials (ASTM), 2008. Standard Test Methods for Sulfur in the Analysis Sample of Coal and Coke Using High-Temperature Tube Furnace Combustion Methods ASTM D 4239.

Anghinoni, L., Zhao, L., Ji, D., Pan, H., 2019. Time series trend detection and forecasting using complex network topology analysis. Neural Network. 117, 295–306.

Assine, M.L., 1992. Análise estratigráfica da Bacia do Araripe, Nordeste do Brasil. Rev. Bras. Geociencias 22 (3), 289–300.

Assine, M.L., 2007. Bacia do Araripe. Boletim de Geociências da Petrobras. Rio de Janeiro 15 (2), 371–389.

Berger, A., 1977. Support of the astronomical theory of climatic change. Nature 268, 44–45.

Berger, A., 1978. Long-term variations of caloric insolation resulting from the earth's orbital elements. Quat. Res. 9, 139–167.

Berger, A., 1988. Milankovitch theory and climate. Rev. Geophys. 26, 624–657.

Berger, A., Loutre, M.F., Laskar, J., 1992. Stability of the astronomical frequencies over the Earth's history for paleoclimate studies. Science 255, 560–566.

Beurlen, K., 1962. A geologia da Chapada do Araripe. Academia Brasileiro de Ciências 34 (3), 365–370.

Beurlen, K., 1971. Bacias sedimentares do Bloco Brasileiro. Estud. Sedimentol. 1 (2), 9–31.

Bradley, W.H., 1929. The Varves and Climate of the Green River Epoch. U.S. Geological Survey Professional Paper. 158-E, pp. 87–110.

Cunha, A.A.S., Azambuja Filho, N.C., 2005. Análise da periodicidade dos folhelhos negros do poço DSDP-520 (Bacia de Angola): um estudo comparativo entre a análise spectral utilizando harmônicos e wavelet. Rev. Bras. Geociencias 35, 25–32.

Flugel, E., 2004. Microfacies of Carbonate Rocks Analysis Interpretation and Application, 976.

Gaspary, J., Anjos, N.F.R., 1964. Estudo hidrogeológico de Juazeiro do Norte, Ceará. Série Hidrogeológica 3, 25.

Gilbert, G.K., 1895. Sedimentary measurement of Cretaceous time. J. Geol. 3 (2), 121–127.

Glenn, C.R., Kelts, K., 1991. Sedimentary rhythms in lake deposits. In: Einsele, Gerhard, Ricken, Werner, Seilacher, Adolf (Eds.), 1991. Cycles and Events in Stratigraphy. Springer-Verlag, Berlin, pp. 188–221.

Hodell, D.A., Brenner, M., Curtis, J.H., Guilderson, T., 2001. Solar forcing of drought frequency in the Maya Lowlands. Science 292, 1367–1370.

Kern, A.K., Harzhauser, M., Piller, W.E., Mandic, O., Soliman, A., 2012. Strong evidence for the influence of solar cycles on a Late Miocene lake system revealed by biotic and abiotic proxies. Paleogreogr. Paleoclimatol. Palaeocol. 329–330, 124–136.

Ludecke, H.J., Weiss, C.O., Hempelmann, A., 2015. Paleoclimate forcing by the solar De Vries/Suess cycle. Clim. Past 11, 279–305.

Mabesoone, J.M., Tinoco, I.M., 1973. Paleoecology of the Aptian Santana formation (Northeastern Brazil). Paleogreogr. Paleoclimatol. Palaeocol. 14 (2), 97–118.

Menezes, T.R., Mendonça Filho, J.G., Araujo, C.V., Souza, I.V.A.F., Mendonça, J.O., 2008. Fácies orgânica: conceitos, métodos e estudos de casos na indústria do petróleo. Rev. Bras. Geociencias 38 (2), 80–96.

Neumann, V.H.D.M.L., 1999. Estratigrafía, sedimentología, geoquímica y diagénesis de los sistemas lacustres Aptiense-Albienses de la Cuenca de Araripe (Noreste de Brasil). PhD Thesis. Barcelona University, 233.

Novello, V.F., Cruz, F.W., Karmann, I., Burns, S.J., Stríkis, N.M., Vuille, M., Cheng, H., Edwards, R.L., Santos, R.V., Frigo, E., Barreto, E.A.S., 2012. Multidecadal climate variability in Brazil's Nordeste during the last 3000 years based on speleothem isotope records. Geophys. Res. Lett. 39. L23706, 6.

Oliveira, A.D., Mendonça-Filho, J.G., Carvalho, M.A., Menezes, T.R., Lana, C.C., Brenner, W.W., 2004. Novo método de preparação palinológicas para aumentar a recuperação de dinoflagelados. Rev. Bras. Palaontol. 7 (2), 169–175.

Perlmutter, M.A., de Azambuja Filho, N.C., 2005. Cyclostratigraphy. In: Koutsoukos, E.A. M. (Ed.), Applied Stratigraphy. Topics in Geobiology, vol. 23. Springer, Dordrecht, pp. 301–338. https://doi.org/10.1007/1-4020-2763-X_14.

Ponte Filho, F.C., 1992. Análise geohistórica do poço 2-AP-1-CE, Bacia do Araripe. In: 2° Simpósio sobre as Bacias Cretácicas Brasileiras, pp. 85–89.

Ponte, F.C., Appi, C.J., 1990. Proposta de revisão da coluna litoestratigráfica da Bacia do Araripe. In: 36° Congresso Brasileiro de Geologia, vol. 1, pp. 211–226.

Priestley, M.B., 1981. Spectral Analysis and Time Series. Academic Press Inc, New York, 890.

Raspopov, O.M., Dergachev, V.A., Esper, J., Kozyreva, O.V., Frank, D., Ogurtsov, M., Kolstrom, T., Shao, X., 2008. The influence of the de Vried (~200-year) solar cycle on climate variations: results from the Central Asian Mountains and their global link. Paleogreogr. Paleoclimatol. Palaeocol. 259 (1), 6–16.

Rayner, J.N., 2001. Spectral analysis. International Encyclopedia of the Social & Behavioral Sciences, pp. 14861–14864.

Regali, M.S.P., Uesugui, N., Santos, A.S., 1974. Palinologia dos sedimentos meso-cenozóicos do Brasil (I). Boletim Técnico da Petrobras, Rio de Janeiro 17 (3), 177–191.

Rios-Netto, A.M., Paula-Freitas, A.B.L., Carvalho, I.S., Regalli, M.S.P., Borghi, L., Freitas, F.I., 2012. Formalização estratigráfica do Membro Fundão, Formação Rio da Batateira, Cretáceo Inferior da Bacia do Araripe, Nordeste do Brasil. Rev. Bras. Geociencias 42 (2), 281–292.

Ruddiman, W.F., 2008. Earth's Climate: Past and Future. W.H. Freeman and Company, New York, 412p.

Schimmelmann, A., Lange, C.B., Meggers, B.J., 2003. Palaeoclimatic and archaeological evidence for a ~200-yr recurrence of floods and droughts linking California, Mesoamerica and South America over the past 2000 years. Holocene 13, 763–778.

Schumacher, B.A., 2002. Methods for the Determination of Total Organic Carbon (TOC) in Soils and Sediments. U.S. Environmental Protection Agency, Washington, DC, p. 25p. EPA/600/R-02/069 (NTIS PB2003-100822).

Schwarzacher, W., 1989. Milankovitch cycles and the measurement of time. Terra. Nova 1 (5), 405–408.

Schwarzacher, W., 1993. Cyclostratigraphy and the Milankovitch Theory. Elsevier Science Publishers, 207.

Schwarzacher, W., 2000. Repetitions and cycles in stratigraphy. Earth Sci. Rev. 50, 51–75.

Seidenglanz, A., Prange, M., Varma, V., Schulz, M., 2012. Ocean temperature response to idealized Gleissberg and de Vries solar cycles in a comprehensive climate model. Geophys. Res. Lett. 39. L22602, 6.

Silva, J.G.R., Azambuja Filho, N.C., 2005. Cicloestratigrafia do Eopermiano – estudo de caso no Grupo Itararé, Bacia do Paraná (parte 2): evidências de indução astronômica (orbital e solar) no clima e na sedimentação. Rev. Bras. Geociencias 35, 77–106.

Strasser, A., Hilgen, F., Heckel, P., 2006. Cyclostratigraphy – concepts, definitions, and applications. Newsl. Stratigr. 42 (2), 75–114.

Suess, H.E., 1980. The radiocarbon record in tree rings of the last 8000 years. Radiocarbon 22 (2), 200–209.

Wagner, G., Beer, J., Masarik, J., Muscheler, R., 2001. Presence of the solar de Vries cycle (~205 years) during the last ice age. Geophys. Res. Lett. 28 (2), 303–306.

Walker, K.F., Likens, G.E., 1975. Meromixis and a reconsidered typology of lake circulation patterns. Verhandlungen der Internationalen Vereinigung für Theoretische und Angewandte Limnologie 19, 442–458.

Weedon, G.P., 2003. Time Series Analysis and Cyclostratigraphy Examining Stratigraphic Records of Environmental Cycles. Cambridge University Press, 259.